Comput. Methods Appl. Mech. Engrg. 197 (2008) 4549–4558

Contents lists available at ScienceDirect

Comput. Methods Appl. Mech. Engrg.

journal homepage: www.elsevier.com/locate/cma

Fully automatic *hp* adaptive finite element method for the Stokes problem in two dimensions

Pawel Matuszyk [a], Maciej Paszyński [b,*]

[a] Department of Applied Computer Science and Modelling, AGH University of Science and Technology, al. Mickiewicza 30, 30-059 Kraków, Poland
[b] Department of Computer Science, AGH University of Science and Technology, al. Mickiewicza 30, 30-059 Kraków, Poland

ARTICLE INFO

Article history:
Received 24 February 2008
Received in revised form 15 May 2008
Accepted 23 May 2008
Available online 10 June 2008

Keywords:
Finite element method
Stokes problem
Automatic *hp*-adaptation
Stabilization

ABSTRACT

The paper is devoted to the solution of the Stokes problem using a self-adaptive *hp*-finite element method (*hp*-FEM) in two dimensions. The *hp*-FEM generates a sequence of optimal *hp* refined meshes delivering exponential convergence rates of the numerical error with respect to the number of degrees of freedom (and CPU time). Optimal meshes are generated by performing a sequence of *h* and *p* refinements on an initial mesh provided by the user. The *hp*-strategy is based on the coarse/fine grid paradigm and the minimization of the projection based interpolation (PBI) error. We employ the Hughes–Franca stabilization method for the stabilization of mixed problem with equal-order elements.

1. Introduction

In this paper, we present an extension of the self-adaptive *hp*-finite element method (*hp*-FEM) [7,15,16] that enables reliable solutions of the Stokes problem in two dimensions. There are some *hp* adaptive FE codes implemented for the Stokes problem [9], however, none of them is fully automatic. The codes usually utilize the initial mesh designed to match known singularities. The *hp* refinement process in these codes is guided on the basis of the knowledge of the exact solution, or the expected location of singularities. The *hp*-FEM code is fully automatic and can be utilized for any arbitrary initial mesh without any knowledge about the location of singularities. The *hp*-FEM code incorporates triangular P_p and quadrilateral Q_p elements ($1 \leqslant p \leqslant 8$) with hierarchical shape functions, and enables the use of 1-irregular meshes (with "hanging" nodes). It allows to solve a system of n partial differential equations (PDEs). It is possible to obtain the vector solution with accuracy prescribed in terms of the energy norm involving all components. An arbitrary initial mesh, prescribed by the user is either h, p or *hp* refined, in such a way that the mesh is optimal for all components of the solution.

The need of approximation of two continuous fields (vector velocity field $\mathbf{u}$, and scalar pressure field p) and the crucial assumption of performing minimal changes in the code forces us to use the equal-order approximation (Q_p/Q_p) for the velocity and pressure. This implies the necessity of using a stabilization technique to overcome limitations imposed on FE spaces by the famous Ladyzhenskaya–Babuśka–Brezzi (LBB) condition [4]. During the last three decades, many stabilization techniques were proposed. In this work, the Hughes–Franca stabilization method [11,10] is used to stabilize a mixed formulation for the stationary Stokes problem.

An efficient implementation for the linear Stokes problem in the *hp*-FEM code provides a starting point for the implementation of a nonlinear Stokes problem. The non-linear formulation will enable the quasi-stationary rigid-viscoplastic model to be utilized in simulation of metal forming processes [13,14].

2. Problem formulation

2.1. Strong form of the Stokes problem

Consider a bounded flow region $\Omega \subset \mathbb{R}^2$ with a Lipschitz boundary $\Gamma = \partial\Omega$ decomposed into two parts: Γ_D where the fluid velocity $\mathbf{u}_D$ is prescribed, and Γ_N where boundary traction $\mathbf{t}$ is given. One has to find a pair $(\mathbf{u}, p)$ which satisfies:

$$\begin{aligned} -\nabla\cdot\boldsymbol{\sigma}(\mathbf{u}) &= \rho\mathbf{b} && \text{in } \Omega,\\ \nabla\cdot\mathbf{u} &= 0 && \text{in } \Omega,\\ \mathbf{u} &= \mathbf{u}_D && \text{on } \Gamma_D,\\ \mathbf{n}\cdot\boldsymbol{\sigma}(\mathbf{u}) &= \mathbf{t} && \text{on } \Gamma_N,\\ \boldsymbol{\sigma}(\mathbf{u}) &= 2\mu\dot{\boldsymbol{\varepsilon}}(\mathbf{u}) - p\mathbf{I} && \text{in } \Omega, \end{aligned} \tag{2.1}$$

where $\mathbf{b}$ is a given body force defined in Ω, $\boldsymbol{\sigma}(\mathbf{u})$ is the Cauchy stress tensor, p is the hydrostatic pressure, $\mathbf{s}(\mathbf{u}) = 2\mu\dot{\boldsymbol{\varepsilon}}(\mathbf{u})$ is the deviatoric stress,

* Corresponding author.
E-mail addresses: pjm@agh.edu.pl (P. Matuszyk), paszynsk@agh.edu.pl (M. Paszyński).

0045-7825/$ - see front matter © 2008 Elsevier B.V. All rights reserved.
doi:10.1016/j.cma.2008.05.027

$$\dot{\varepsilon}(\mathbf{u}) = \frac{1}{2}\left(\nabla\mathbf{u} + \nabla^{\mathrm{T}}\mathbf{u}\right)$$

is the strain rate tensor, ρ is the fluid density, $\mathbf{I}$ is the identity tensor, and μ is the fluid dynamic viscosity. The first equation represents momentum balance, whilst the second incompressibility of the fluid. The last equation represents the constitutive relation between the stress and the strain rate.

2.2. Weak form of the Stokes problem

Multiplying the first equation in (2.1) by velocity test functions $\mathbf{v}$ coming from the space

$$\mathbf{V} = \{\mathbf{v} \in \mathbf{H}^1(\Omega) : \mathbf{v} = 0 \quad \text{on} \quad \Gamma_D\} \tag{2.2}$$

and multiplying the second equation in (2.1) by pressure test functions $q \in Q = L^2(\Omega)$, after integrating by parts and incorporating the boundary conditions on Γ, we obtain the following weak formulation of the Stokes problem.

Find $(\mathbf{u}, p) \in (\mathbf{u}_D + \mathbf{V}) \times Q$ satisfying:

$$\begin{aligned}
&\int_\Omega 2\mu\dot{\varepsilon}(\mathbf{u}) : \dot{\varepsilon}(\mathbf{v})\,\mathrm{d}\Omega - \int_\Omega p\nabla\cdot\mathbf{v}\,\mathrm{d}\Omega \\
&\quad = \int_\Omega \rho\mathbf{b}\cdot\mathbf{v}\,\mathrm{d}\Omega + \int_{\Gamma_N} \mathbf{t}\cdot\mathbf{v}\,\mathrm{d}\Gamma_N \quad \forall\mathbf{v}\in\mathbf{V}, \\
&\quad - \int_\Omega q\nabla\cdot\mathbf{u}\,\mathrm{d}\Omega = 0 \quad \forall q \in Q.
\end{aligned} \tag{2.3}$$

To solve such a mixed problem one has to apply special finite elements with different orders of approximation for velocity and pressure fields, which satisfy the discrete Babuška–Brezzi [4] condition. Limited by the existing *hp*-FEM code, we are bounded to use finite elements with the same order for velocity and pressure. Thus, we employ a stabilization technique. For our purpose, the Hughes–Franca stabilization seems to be adequate [10,11].

2.3. Stabilization of the weak form of the Stokes problem

Let $\mathscr{T}_{hp}$ be a triangulation of the domain Ω. The Hughes–Franca method [11] starts by selecting a test function $\mathbf{w}$ of the form

$$\mathbf{w} = \mathbf{v} + \tau_K\nabla q, \tag{2.4}$$

where $\mathbf{v} \in \mathbf{V}, q \in Q$, and τ_K is the stabilization parameter defined element-wise as

$$\tau_K = \frac{\alpha}{2\mu}\frac{\max\{h_K^x, h_K^y\}^2}{\max\{p_K^x, p_K^y\}},$$

where $\{h_K^x, h_K^y\}$ are element dimensions and (p_K^x, p_K^y) are polynomial orders of approximation over an element K in the horizontal and vertical direction, respectively, and α is a non-dimensional positive constant, called stability parameter.

Multiplying Eq. $(2.1)_1$ with test function $\mathbf{w}$, and integrating over Ω we obtain:

$$-\int_\Omega \nabla\cdot\boldsymbol{\sigma}(\mathbf{u})\cdot\mathbf{w}\,\mathrm{d}\Omega = \int_\Omega \rho\mathbf{b}\cdot\mathbf{w}\,\mathrm{d}\Omega. \tag{2.5}$$

In accordance with the Hughes–Franca method [11], the second term of (2.4) is understood element-wise only. Thus (2.5) transforms to:

$$\begin{aligned}
&-\int_\Omega \nabla\cdot\boldsymbol{\sigma}(\mathbf{u})\cdot\mathbf{v}\,\mathrm{d}\Omega - \sum_{K\in\mathscr{T}_{hp}}\int_K \tau_K\nabla q\cdot\nabla\cdot\boldsymbol{\sigma}(\mathbf{u})\,\mathrm{d}K \\
&\quad = \int_\Omega \rho\mathbf{b}\cdot\mathbf{v}\,\mathrm{d}\Omega + \sum_{K\in\mathscr{T}_{hp}}\int_K \tau_K\nabla q\cdot\rho\mathbf{b}\,\mathrm{d}K.
\end{aligned}$$

Integrating the first term by parts, applying boundary conditions and using constitutive Eq. $(2.1)_5$, we obtain

$$\begin{aligned}
&\int_\Omega 2\mu\dot{\varepsilon}(\mathbf{u}) : \dot{\varepsilon}(\mathbf{v})\,\mathrm{d}\Omega - \int_\Omega p\nabla\cdot\mathbf{v}\,\mathrm{d}\Omega \\
&\quad - \sum_{K\in\mathscr{T}_{hp}}\int_K \tau_K\nabla q\cdot(\nabla\cdot\mathbf{s}(\mathbf{u}) - \nabla p)\,\mathrm{d}K \\
&\quad = \int_\Omega \rho\mathbf{b}\cdot\mathbf{v}\,\mathrm{d}\Omega + \int_{\Gamma_N}\mathbf{t}\cdot\mathbf{v}\,\mathrm{d}\Gamma_N + \sum_{K\in\mathscr{T}_{hp}}\int_K \tau_K\nabla q\cdot\rho\mathbf{b}\,\mathrm{d}K.
\end{aligned} \tag{2.6}$$

Next, we multiply the incompressibility equation $(2.1)_2$ with test function q, integrate over the domain and incorporate (2.6) to obtain the final equation

$$\begin{aligned}
&\int_\Omega 2\mu\dot{\varepsilon}(\mathbf{u}) : \dot{\varepsilon}(\mathbf{v})\,\mathrm{d}\Omega - \int_\Omega p\nabla\cdot\mathbf{v}\,\mathrm{d}\Omega \\
&\quad = \int_\Omega \rho\mathbf{b}\cdot\mathbf{v}\,\mathrm{d}\Omega + \int_{\Gamma_N}\mathbf{t}\cdot\mathbf{v}\,\mathrm{d}\Gamma_N \quad \forall\mathbf{v}\in\mathbf{V}, \\
&\int_\Omega q\nabla\cdot\mathbf{u}\,\mathrm{d}\Omega + \sum_{K\in\mathscr{T}_{hp}}\int_K \tau_K\nabla q\cdot\nabla p\,\mathrm{d}K \\
&\quad = \sum_{K\in\mathscr{T}_{hp}}\int_K \tau_K\nabla q\cdot\rho\mathbf{b}\,\mathrm{d}K \\
&\qquad + \sum_{K\in\mathscr{T}_{hp}}\int_K \tau_K\nabla q\cdot(\nabla\cdot\hat{\mathbf{s}}(\mathbf{u}))\,\mathrm{d}K \quad \forall q\in Q.
\end{aligned} \tag{2.7}$$

Following [11,10,13], in the formulation above one assumes that the last term in $(2.7)_2$ is treated as an additional force acting on the system. This allows to avoid calculations of the second derivatives of the velocity field ($\nabla\cdot\mathbf{s} = 2\mu\nabla\cdot\dot{\varepsilon}$). Thus, unknown $\mathbf{s}$ (which is a function of the second-order derivatives of the velocity field) is replaced by $\hat{\mathbf{s}}$ (reconstructed on the basis of the current velocity field). We emphasize that this term is understood only element-wise, i.e. the non-integrable Dirac's type terms corresponding to inter-element boundaries are neglected. In the case of linear elements, the term vanishes, while use of higher order elements implies the necessity of using deviator $\mathbf{s}$ for the reconstruction on the basis of the velocity field and the constitutive relation. We follow the method of stress-deviator reconstruction proposed in Ref. [12].

Remark 1. Solution of (2.7) combines a direct solution of system (2.7) with simple iterations with respect to the "additional force" term in Eq. $(2.7)_2$.

2.4. The discrete problem

The ultimate discrete problem is obtained by taking finite-dimensional subspaces $\mathbf{V}_{hp} \subset \mathbf{V}$ and $Q_{hp} \subset Q$ and rewriting (2.7) as follows:

find $(\mathbf{u}_{hp}, p_{hp}) \in (\mathbf{u}_D + \mathbf{V}_{hp}) \times Q_{hp}$ satisfying:

$$\begin{aligned}
&\int_\Omega 2\mu\dot{\varepsilon}(\mathbf{u}_{hp}) : \dot{\varepsilon}(\mathbf{v}_{hp})\,\mathrm{d}\Omega - \int_\Omega p_{hp}\nabla\cdot\mathbf{v}_{hp}\,\mathrm{d}\Omega \\
&\quad = \int_\Omega \rho\mathbf{b}\cdot\mathbf{v}_{hp}\,\mathrm{d}\Omega + \int_{\Gamma_N}\mathbf{t}\cdot\mathbf{v}_{hp}\,\mathrm{d}\Gamma_N \quad \forall\mathbf{v}_{hp}\in\mathbf{V}_{hp}, \\
&\int_\Omega q_{hp}\nabla\cdot\mathbf{u}_{hp}\,\mathrm{d}\Omega + \sum_{K\in\mathscr{T}_{hp}}\int_K \tau_K\nabla q_{hp}\cdot\nabla p_{hp}\,\mathrm{d}K \\
&\quad = \sum_{K\in\mathscr{T}_{hp}}\int_K \tau_K\nabla q_{hp}\cdot\rho\mathbf{b}\,\mathrm{d}K + \sum_{K\in\mathscr{T}_{hp}}\int_K \tau_K\nabla q_{hp} \\
&\qquad \times(\nabla\cdot\hat{\mathbf{s}}(\mathbf{u}_{hp}))\,\mathrm{d}K \quad \forall q_{hp}\in Q_{hp}.
\end{aligned} \tag{2.8}$$

We multiply $(2.8)_2$ by factor -1 in order to obtain a symmetric formulation.

2.5. Deviatoric stress reconstruction

Reconstruction of the components of tensor $\hat{\mathbf{s}}$ is performed for each element separately by performing a local L^2-projection. Over

each element, each component $\hat{s}^{ij}$ of the tensor $\hat{\mathbf{s}}$ is expressed in terms of the element shape functions ϕ_k and unknown nodal values $\hat{s}^{ij}_k$ (to be reconstructed):

$$\hat{s}^{ij} = \sum_k \phi_k \hat{s}^{ij}_k.$$

With s^{ij}_k calculated, the divergence of $\hat{\mathbf{s}}$ can be simply evaluated by means of derivatives of the element shape functions as:

$$\nabla \cdot \hat{\mathbf{s}} = \hat{s}^{ij}_{,i} = \sum_k \phi_{k,i} \hat{s}^{ij}_k.$$

Having an approximated solution $\mathbf{u}_{hp}$ obtained from the previous iterations of the *hp*-FEM, one can reconstruct nodal components of the deviatoric stress by solving three (we have three components of the tensor $\hat{\mathbf{s}}$) dense systems of linear equations with the same mass matrix:

$$\mathbf{M} \cdot \hat{\mathbf{s}}^{ij} = \mathbf{R}^{ij}, \quad \hat{\mathbf{s}}^{ij} = \{\hat{s}^{ij}_k\}, \tag{2.9}$$

where

$$\mathbf{M}_{pq} = \int_K \phi_p \phi_q \, \mathrm{d}K, \quad \mathbf{R}^{ij}_p = \int_K s^{ij}(\mathbf{u}_{hp}) \, \mathrm{d}K = \int_K 2\mu \dot{\varepsilon}^{ij}(\mathbf{u}_{hp}) \phi_p \, \mathrm{d}K.$$

Thus, for each finite element, the Cholesky decomposition $\mathbf{L}\mathbf{L}^{\mathrm{T}}$ for the matrix $\mathbf{M}$ is done only once, and the three systems of linear equations (2.9) with different right-hand sides $\mathbf{R}^{ij}$ are solved.

We treat *hp*-adaptation process as an iterative procedure generating finer and finer solutions. In the case of deviatoric stress reconstruction, this iterative procedure can be utilized in order to reconstruct the "additional force" term in $(2.7)_2$ (cf. Remark 1). The deviatoric stress is calculated successively element-wise in each *hp*-iteration, based on the velocity field $\mathbf{u}_{hp}$ calculated in the previous *hp*-iteration. Our numerical experiments indicate that it is sufficient to start with a zero velocity field in the first *hp*-iteration, which is usually performed usually with a very coarse mesh.

3. Automatic *hp* adaptivity

The self-adaptive *hp*-FEM described in detail in [5,6] can be summarized as follows. The algorithm is based on the two grid paradigm: a coarse *hp* mesh, and a fine *hp* mesh that is obtained from the coarse one by performing a global *hp* refinement. This means that each finite element of the coarse grid is broken into four new son elements, and the polynomial order of approximation (p^x_K, p^y_K) is uniformly raised by one to $(p^x_K + 1, p^y_K + 1)$ over each finite element K. The fine grid solution $(\mathbf{u}_{h/2,p+1}, p_{h/2,p+1}) \in \mathbf{V}_{h/2,p+1} \times Q_{h/2,p+1}$ is used then to guide optimal refinements of the coarse grid to produce the next optimal coarse grid. The fine grid solution is projected separately onto each coarse grid element and onto a nested sequence of meshes that is locally embedded in the fine grid. For each coarse grid element, the sequence is built dynamically by testing all possible types of local *h*-refinements, and selecting the one that provides the maximum error decrease rate

$$r_{\mathrm{opt}} = \max_{\widetilde{\mathbf{w}} \in \widetilde{\mathbf{V}}} \max_{\widetilde{q} \in \widetilde{Q}} \frac{\sqrt{e_u^2 + e_p^2}}{\delta N_{\mathrm{DOF}}}, \tag{3.10}$$

where

$$\mathbf{V}_{hp} \subseteq \widetilde{\mathbf{V}} \subseteq \mathbf{V}_{h/2,p+1} \quad \text{is a trial velocity space,}$$

$$Q_{hp} \subseteq \widetilde{Q} \subseteq Q_{h/2,p+1} \quad \text{is a trial pressure space,}$$

$$e_u = |\mathbf{u}_{h/2,p+1} - \mathbf{u}_{hp}|^2_1 - |\mathbf{u}_{h/2,p+1} - \widetilde{\mathbf{w}}|^2_1, \tag{3.11}$$

$$e_p = \|p_{h/2,p+1} - p_{hp}\|^2_0 - \|p_{h/2,p+1} - \widetilde{q}\|^2_0, \tag{3.12}$$

where δN_{DOF} is the number of added degrees of freedom during the refinement, $(\widetilde{\mathbf{w}}, \widetilde{q}) \in \widetilde{\mathbf{V}} \times \widetilde{Q}$ is the solution of the proposed refinement strategy, $|\mathbf{u}_{h/2,p+1} - \mathbf{u}_{hp}|_1$ is the relative error estimation over the current coarse mesh with respect to the fine mesh measured in the $\mathbf{H}^1$ semi-norm, and $|\mathbf{u}_{h/2,p+1} - \widetilde{\mathbf{w}}|_1$ is the relative error estimation for the refinement strategy proposed for the finite element with respect to the fine mesh. For the pressure we utilize L^2 norm.

Specifically, the algorithm consists of two steps [5,6], dealing with edges, and element interiors. The optimal refinement from the first step provides the minimal refinement for the next. The final optimal refinements for elements are possibly upgraded in order to maintain the 1-irregularity rule. The optimal refinements are finally executed over the coarse grid in order to generate the next optimal coarse grid.

4. Implementation

The implementation of the *hp* adaptivity for the stationary Stokes problem is based on the fully automatic 2D FEM package [5,7,15,16] for elliptic problems. The package was designed for solving scalar elliptic problems, and the decisions about optimal h, p or *hp* refinements were made based on the H^1 Sobolev semi-norm, instead of the full H^1 norm. The following modifications were performed to enable solution of the stationary Stokes problem:

- We re-implemented all procedures constructing local element matrices in order to support the stabilized Stokes formulation. It includes the following procedures: imposing the boundary conditions and building local stiffness matrices. We also added the procedure of performing local L^2 projections for the calculation of components of the reconstructed deviatoric stress tensor.
- We restricted the H^1 Sobolev semi-norm to the velocity field components. We utilized the L^2 norm as a relative error estimator for the pressure component (Eq. (3.10)).

We use the H^1 semi-norm for the velocity component instead of a more appropriate energy norm. This is motivated by the equivalence of these two norms (by virtue of the Korn's inequality).

Fig. 1. Different colors denoting different polynomial orders of approximation. (For interpretation of the references to color in this figure legend, the reader is referred to the web version of this article.)

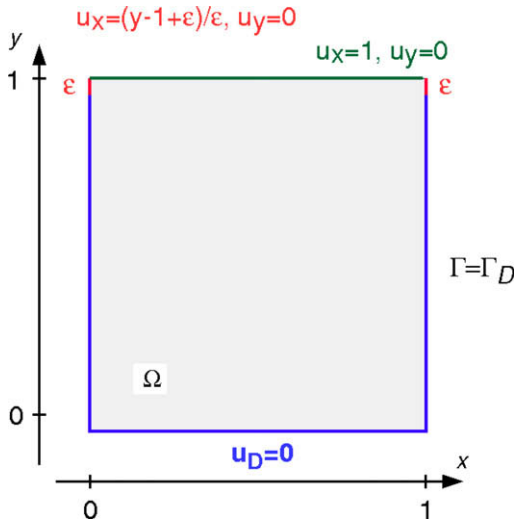

Fig. 2. Definition of geometry in the cavity problem.

5. Results

This section presents numerical results for four selected benchmark problems. The computational meshes generated by the self-adaptive *hp*-FEM utilize polynomials of different orders, which are indicated by different colors as presented in Fig. 1.

The relative error presented in Figs. 8, 10, 11, 16 and 21 is defined by

$$e = \sqrt{e_u^2 + e_p^2}$$

with e_u and e_p given by (3.11) and (3.12). It is defined as the relative error difference between the coarse and fine mesh solutions, with $\mathbf{H}^1$ semi-norm utilized for the velocity components and L^2 norm utilized for the pressure.

5.1. Example 1: driven cavity problem

The cavity flow problem has been solved as the standard benchmark test for the incompressible fluid flow [8]. It models a plane flow of an isothermal fluid in a square lid-driven cavity of size $(0,1)^2$. For our purposes, we selected a fluid dynamic viscosity $\mu = 1$ and a body force $\mathbf{b} = 0$.

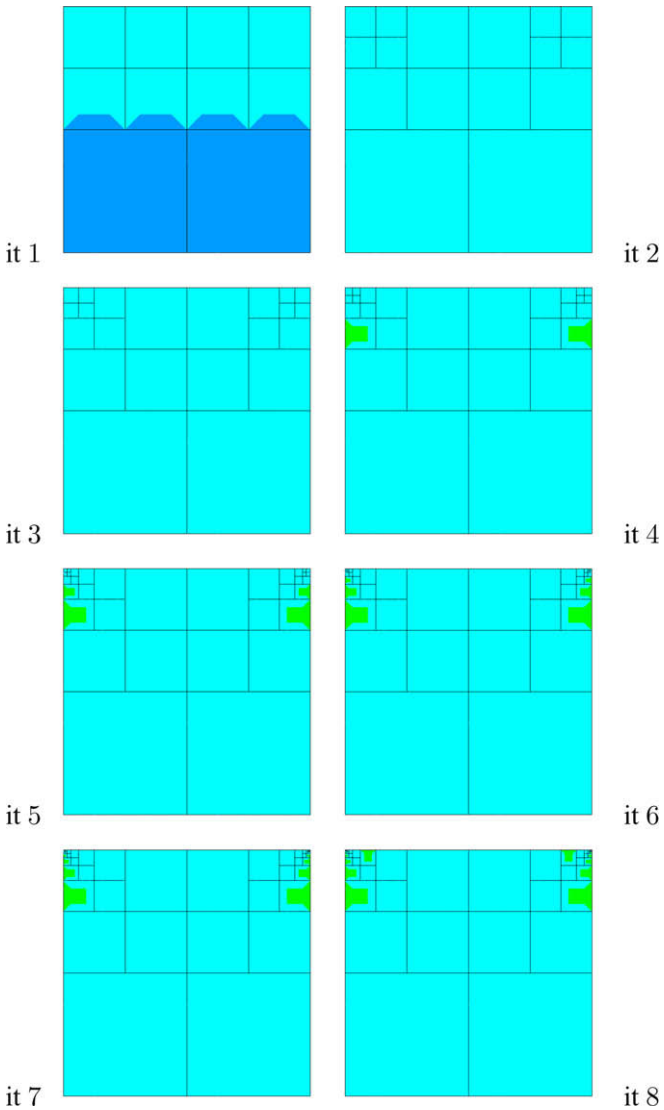

Fig. 3. Cavity problem. Sequence of optimal meshes at iterations 1–8.

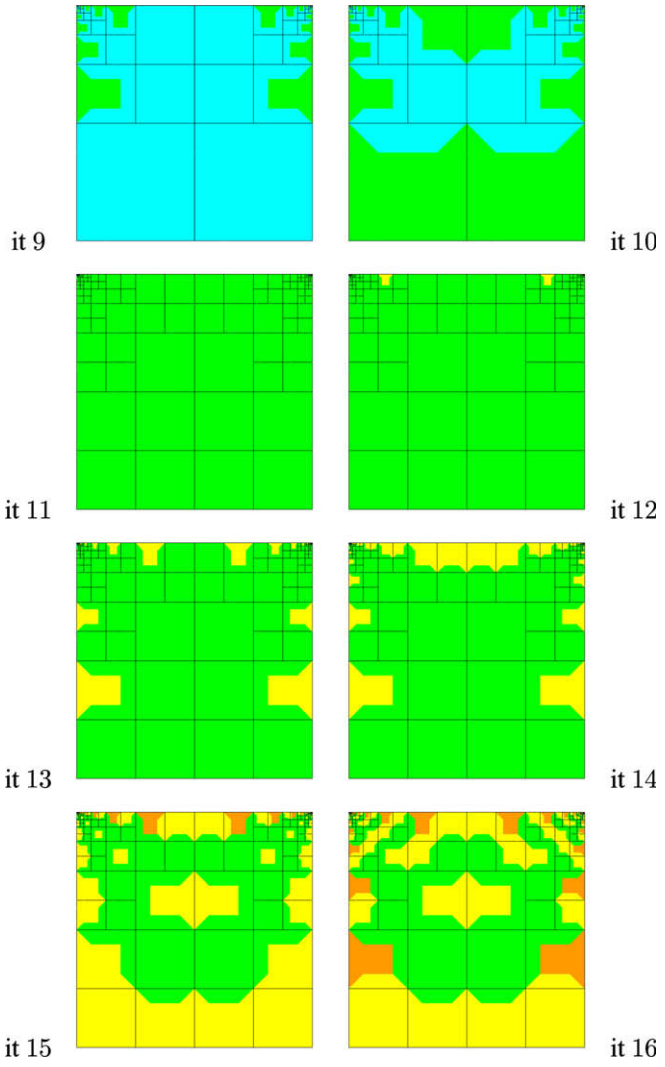

Fig. 4. Cavity problem. Sequence of optimal meshes at iterations 9–16.

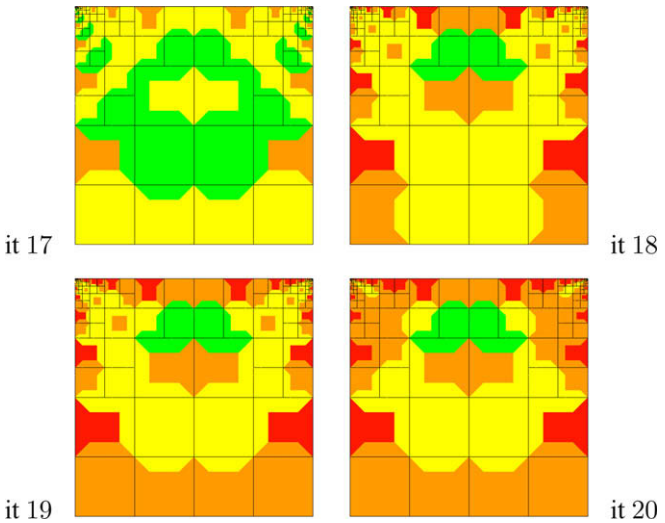

Fig. 5. Cavity problem. Sequence of optimal meshes at iterations 17–20.

To assure uniqueness of the pressure and due to the fact that on the whole boundary Dirichlet conditions are imposed for **u**, the pressure at the point (0.5,0) was set to zero.

The special choice of Dirichlet boundary conditions for **u** (see Fig. 2) the results in discontinuities in the boundary conditions and yields singularities in pressure field at the two upper corner points: (0,1) (where the pressure tends to minus infinity) and (1,1) (where the pressure tends to infinity) [8].

To assure well-posedness of the problem – velocity $\mathbf{u}_{hp}$ must belong to the space $\mathbf{H}^1(\Omega)$ – the Dirichlet data have to belong to the $\mathbf{H}^{1/2}(\Gamma_D)$ space (i.e. if the function on the boundary Γ_D lays in $\mathbf{H}^{1/2}$, it can be extended into Ω to a function that belongs to the space

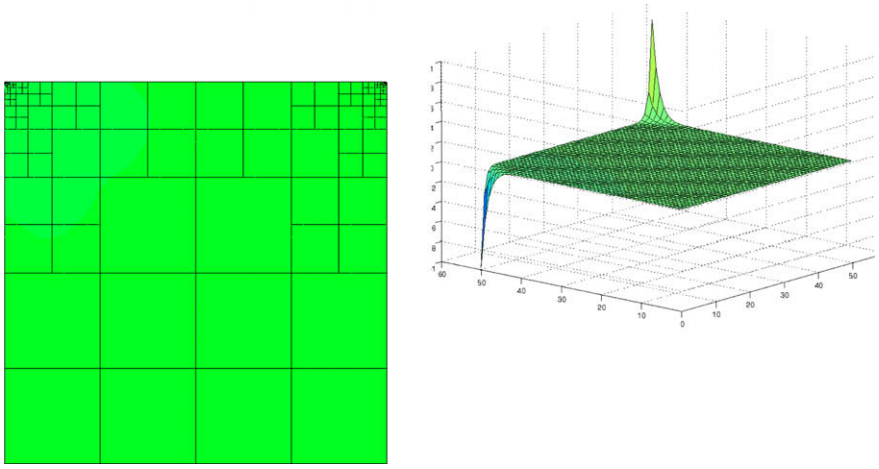

Fig. 6. Pressure calculated for the optimal mesh and the pressure component of exact solution.

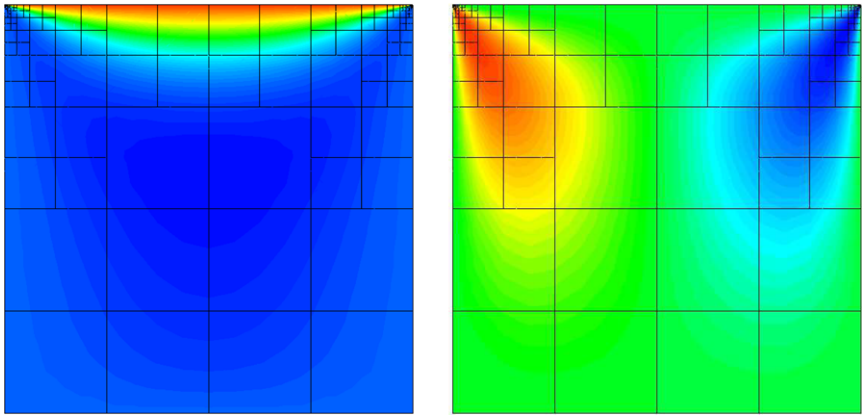

Fig. 7. v_x and v_y components of the velocity field calculated for the optimal mesh.

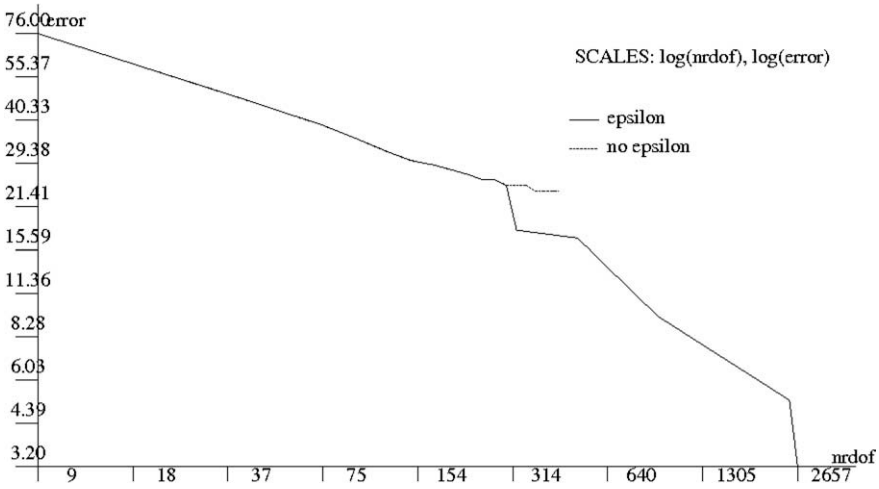

Fig. 8. The comparison of convergence curves for 15 iterations with and without the ε-transition zones.

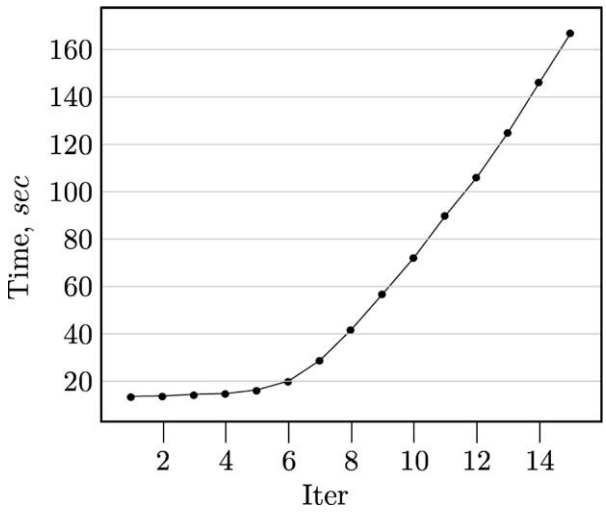

Fig. 9. Execution time of each iteration during the automatic *hp*-adaptation algorithm for cavity problem, starting from 2×2 coarse FE mesh with approximation order $p = 1$.

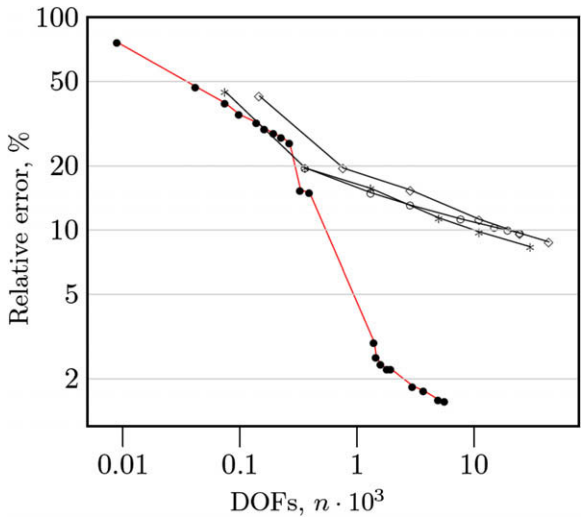

Fig. 11. Convergence curve: norm of error versus number DOFs: automatic *hp* adaptation (•), uniform *h* refinements for approximation order $p = 1$ (○), uniform *h* refinements for $p = 2$ (∗), uniform *h* refinements for $p = 3$ (◊).

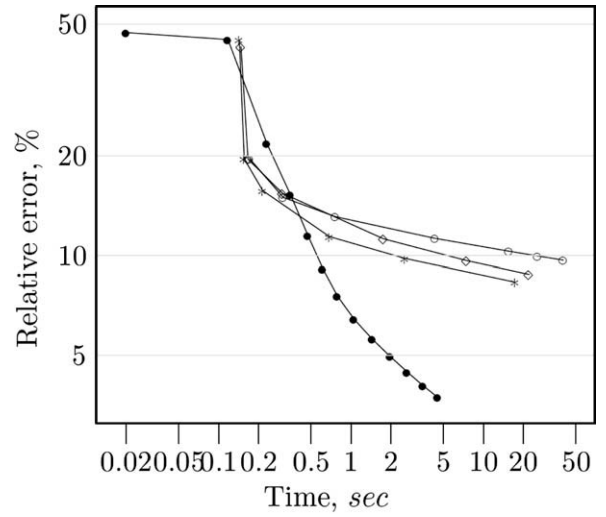

Fig. 10. Relative error versus execution time for different refinement strategies: automatic *hp* adaptation (•), uniform *h* refinements for approximation order $p = 1$ (○), uniform *h* refinements for $p = 2$ (∗), uniform *h* refinements for $p = 3$ (◊).

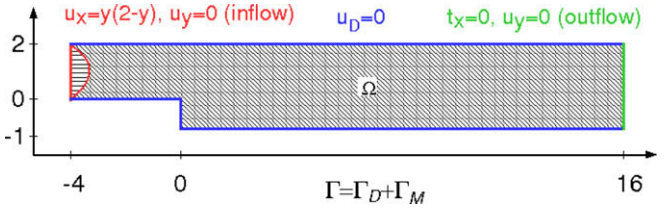

Fig. 12. Definition of the geometry and prescribed boundary conditions for the step problem.

$\mathbf{H}^1(\Omega)$). Therefore, the trace cannot be discontinuous, and ε-transition zones were added accordingly, with the horizontal component of the velocity changing linearly form 0 to 1. The magnitude of the ε parameter controls the "order of singularity" at both top corners. The value $\varepsilon = 10^{-4}$ was taken for the calculations. Taking Dirichlet data coming from a larger space (less smooth functions) implies that the extension to the $\mathbf{H}^1$-function over Ω may not exist and, in consequence, the solution of the problem (2.8) may not exist either.

The sequence of optimal *hp*-meshes is presented in Figs. 3–5. Colors indicate the orders of approximation over particular finite elements.

The automatic *hp* adaptive algorithm captured both known singularities, by performing a sequence of *h* refinements at the corners with singularities, and increasing the polynomial order of approximation in the remaining part of the domain, where the solution is smoother. This corresponds well to the theory [5]. The obtained solution is presented in Figs. 6 and 7.

The necessity for defining the boundary conditions with the ε-transition zones is illustrated in Fig. 8. In the pictures, the convergence curve for 15 iterations with the formulation with ε-transition zones is compared with the convergence curve for 15 iterations with the formulation without the transition zones. The relative error between the coarse and fine mesh solutions measured in the H^1 semi-norm for the velocity and L^2 norm for the pressure is utilized as the error indicator. The self-adaptive *hp*-FEM strategy for the formulation without transition zones reaches 24.0% accuracy of the solution and is locked, while the *hp*-FEM utilized for the formulation with transition zones goes down to 3.2% relative error, where the simulation has been finished.

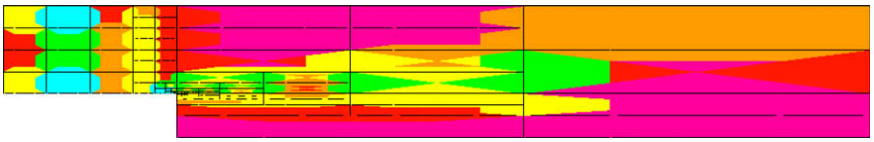

Fig. 13. Optimal mesh obtained for the step problem.

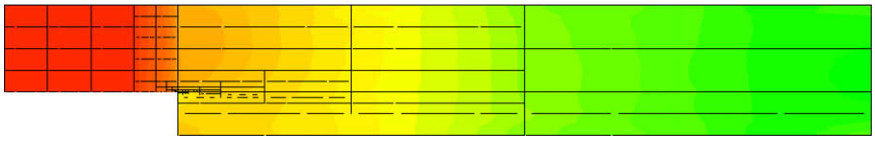

Fig. 14. Step problem. Pressure distribution.

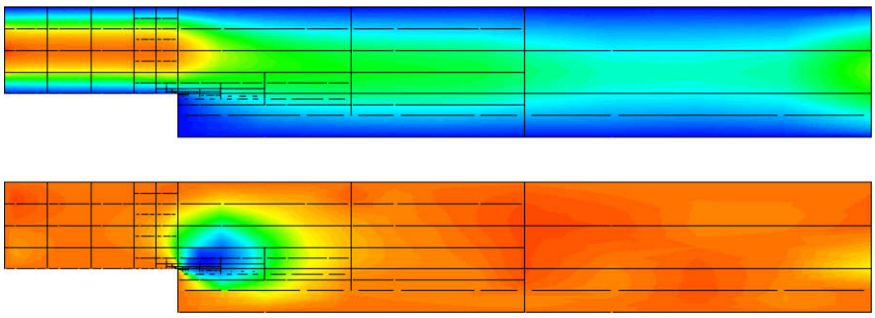

Fig. 15. Step problem. v_x (top) and v_y (bottom) components of the velocity field calculated for the optimal mesh.

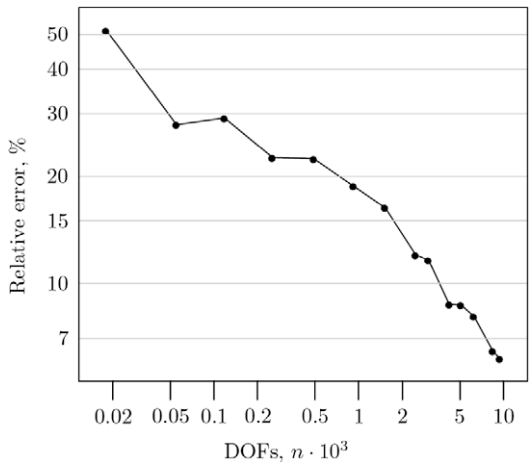

Fig. 16. Step problem. Convergence curve.

5.1.1. Computational cost

To verify the efficiency of the fully automatic 2D *hp* adaptive FEM for the stationary Stokes problem, some numerical experiments were performed for the lid-driven cavity problem.

The code was executed starting from the initial mesh containing four finite elements, with uniform polynomial order of approximation equal to 1. The required accuracy of the solution was 3% relative error. We performed measurements of the execution time for 15 iterations of the *hp*-FEM. The measurements are reported in Fig. 9. We compared the execution time of the self-adaptive *hp*-FEM starting from $p = 12 \times 2$ finite elements mesh, with three uniform h refinement strategies. The uniform h refinement strategy breaks every finite element into four new sons elements at each iteration. We performed three tests with the uniform h refinement. The tests were executed on the initial mesh with $2 \times 2 = 4$ elements meshes, with uniform polynomial orders of approximation set to $p = 2, p = 3$ and $p = 4$, respectively. The relative error for the uniform h refinement strategy was also defined as the $\mathbf{H}^1$ semi-norm difference between the coarse and corresponding fine mesh solutions.

Comparison of the execution times of the automatic *hp*-adaptive algorithm with uniform h refinement strategies for the three mentioned meshes is presented in Fig. 10. We observe that the automatic *hp*-adaptive refinement strategy is much faster and provides less relative error than any uniform h refinement strategy.

We also compared the total execution time necessary to obtain a solution with a relative error equal to 3.2% (453 s) with the execution time of a single iteration (coarse and fine mesh solution) on

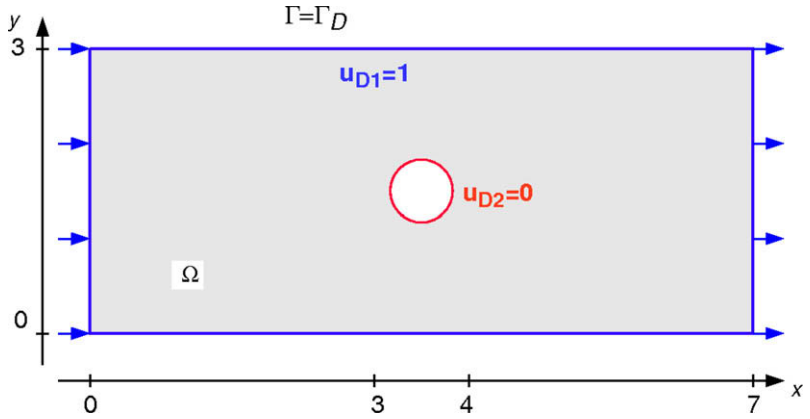

Fig. 17. Definition of the geometry and prescribed boundary conditions for the obstacle problem.

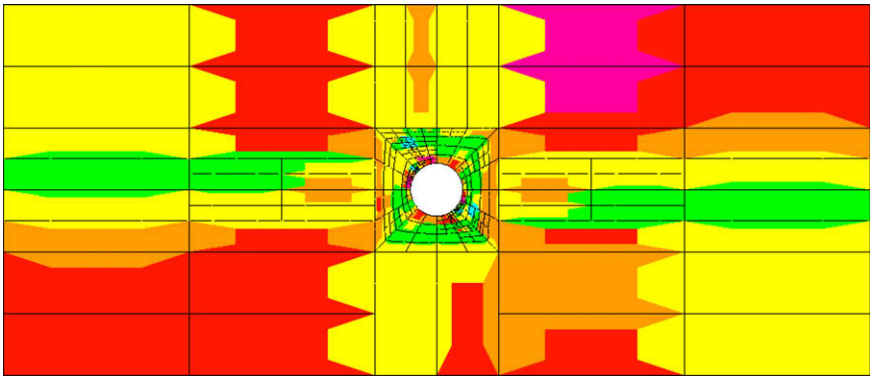

Fig. 18. Optimal mesh obtained for the obstacle problem.

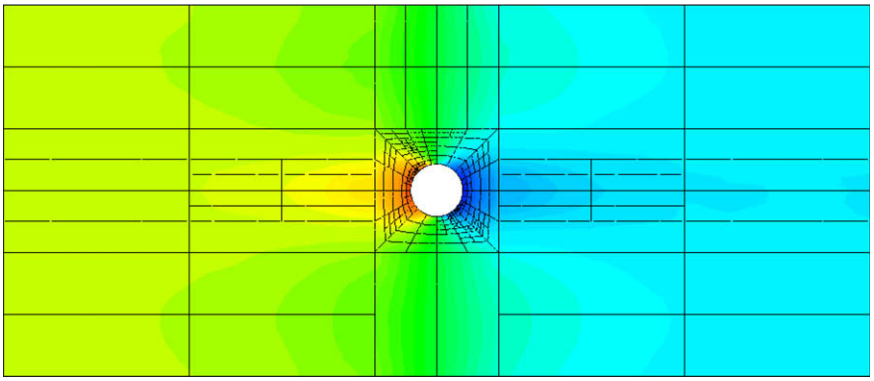

Fig. 19. Obstacle problem. Pressure distribution.

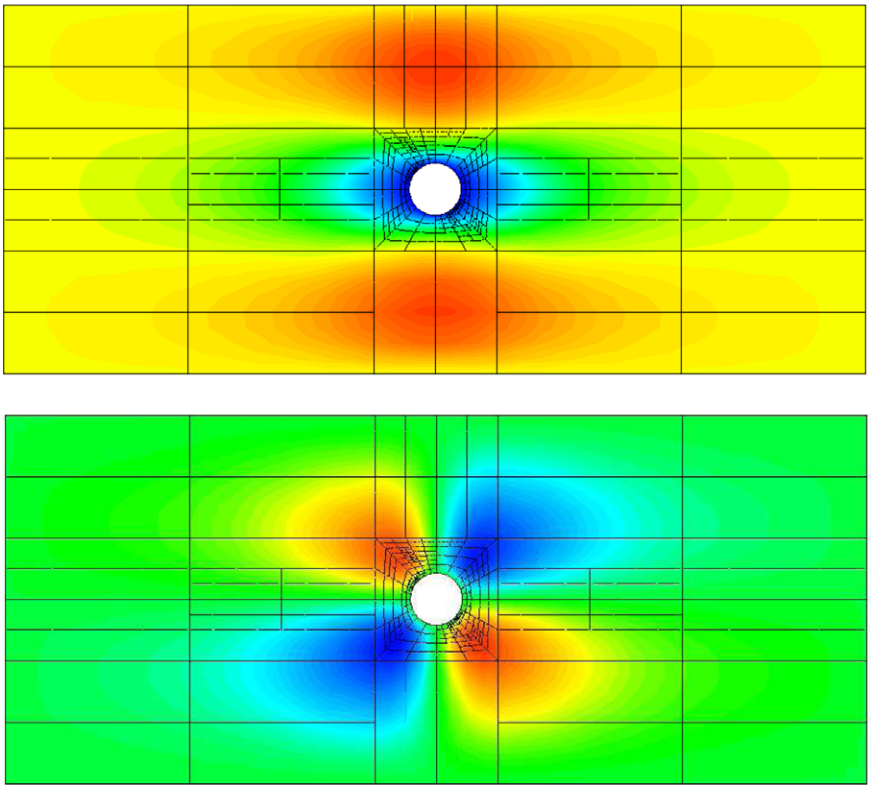

Fig. 20. Obstacle problem. v_x (top) and v_y (bottom) components of the velocity field calculated for the optimal mesh.

the uniform 90×90 $p = 3$ finite elements mesh (4011 s), which provides only a 10.0% relative error of the solution.

The convergence curve for the automatic *hp*-adaptation and *h* version of FEM is presented in Fig. 11. From the experiment, it follows, that the accuracy of the solution over the large uniform 8100 elements esh is significantly worse (10% relative error) than the accuracy obtained after 15 iterations of the automatic *hp* adaptivity, whilst the execution time over the large uniform mesh was nearly 9 times larger.

As one can observe, the self-adaptive *hp*-FE method delivers exponential convergence rates in terms of the relative error versus the number of unknowns, which coincides with the theory [1–3].

The convergence rate deteriorates after obtaining the maximum order of approximation implemented in the code ($p = 8$), and the automatic adaptivity for elements with $p = 8$ switches to *h* adaptivity, which has at most an algebraic convergence rate. The uniform *h* refinements for constant uniform *p* over the entire mesh also delivers algebraic convergence only.

5.2. Example 2: step problem

The geometry and prescribed boundary conditions are presented in Fig. 12. We selected a fluid dynamic viscosity $\mu = 1$, a body force $\mathbf{b} = 0$ and a stabilization coefficient $\alpha = 0.01$. The optimal mesh, pressure distribution and components of the velocity field are presented in Figs. 13–15. Convergence curve obtained for the step problem is presented in Fig. 16.

5.3. Example 3: obstacle problem

The next problem is the obstacle problem. The geometry and prescribed boundary conditions are presented in Fig. 17. Fluid dynamic viscosity $\mu = 1$, body force $\mathbf{b} = 0$ and stabilization coefficient $\alpha = 0.01$ were taken. The optimal mesh, pressure distribution and components of the velocity field are presented in Figs. 18–20. Convergence curve obtained for the obstacle problem is presented in Fig. 21.

The solution to this problem is smooth. Thus, the *p* adaptive method delivers the exponential convergence. The initial mesh utilized for this problem had the uniform order of approximation $p = 2$, in order to properly represent the shape of the circular obstacle. We have observed the exponential convergence within first 5–6 iterations, however the convergence rate deteriorates for further iterations. We believe this is due to the limit of $p = 8$ utilized in the code.

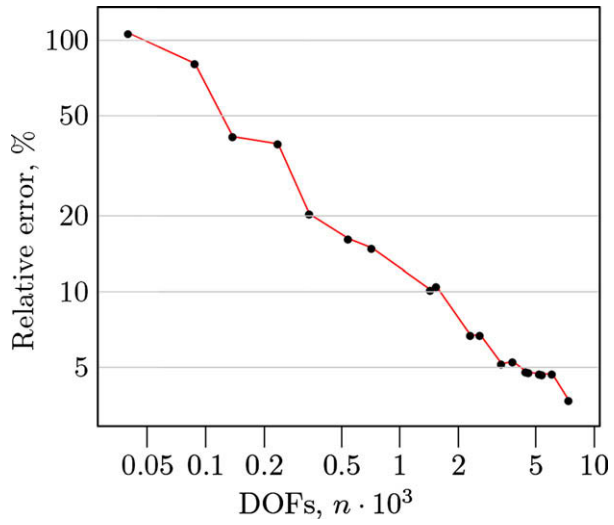

Fig. 21. Obstacle problem. Convergence curve.

6. Conclusions and future work

The automatic *hp* adaptivity is the fastest known adaptation strategy, where the numerical error converges exponentially with respect to the number of degrees of freedom. In other words, other adaptation strategies, such as uniform *h* refinement, starting from an initial mesh with $p = 1$ or $p = 2$ (see Fig. 11) or any other constant *p* as well as automatic *h* adaptivities [5] provide only algebraic convergence. In the other hand, applying the *p* adaptivity only, the exponential convergence is provided for the smooth solutions only. In the case of singularities present in the domain, the convergence of *p* methods deteriorates and becomes algebraic.

- In this paper, we have developed a fully automatic *hp* adaptive FEM code for the stationary 2D Stokes problem stabilized by using Hughes–Francs method.
- The 48% numerical error on the initial mesh was reduced to 3.2% error using 3014-DOF $\times 3$ (there are 2 velocity and one pressure component at each node for the mesh) by performing 15 iterations of the fully automatic 2D *hp*-adaptive FEM algorithm.
- The algorithm has been tested on the cavity flow problem, with the Dirichlet boundary conditions chosen in such a way that it generates two singularities at the two top corners of the domain. To generate an optimal mesh capturing the singularities, a sequence of *h* refinements followed by *p* refinements was produced by the code. The *h* refinements in the directions of singularities reduce the relative error generated by singularities, whilst *p* refinements on the remaining part of the mesh approximates the smooth components of the solution.
- We obtained the exponential convergence of the relative error with respect to the number of DOFs (size of the problem), which coincides with the theoretical results for *hp* adaptivity [1–3].
- The future work may involve application of the code to more challenging problems (with non-linear constitutive model) and extension the code to three dimensions.

Acknowledgement

The financial support of this work under MNiSW Grant No. 3 T08B 055 29 is acknowledged.

References

[1] I. Babuska, B.A. Szabo, I.N. Katz, The *p*-version of the finite element method, SIAM J. Numer. Anal. 18 (1981) 515–545 .
[2] I. Babuska, B. Guo, The *hp*-version of the finite element method, Part I: The basic approximation results, Comput. Mech. 1 (1986) 21–41.
[3] I. Babuska, B. Guo, The *hp*-version of the finite element method, Part II: General results and applications, Comput. Mech. 1 (1986) 203–220.
[4] F. Brezzi, M. Fortin, Mixed and Hybrid Finite Element Methods, Springer-Verlag, Berlin, 1991.
[5] L. Demkowicz, Computing with *hp*-Adaptive Finite Elements: Part I. One- and Two-Dimensional Elliptic and Maxwell Problems, first ed, CRC Press, Boca Raton, FL, 2006.
[6] L. Demkowicz, J. Kurtz, D. Pardo, M. Paszyński, W. Rachowicz, A. Zdunek, Computing with hp-Adaptive Finite Elements: Part II. Frontiers. Three Dimensional Elliptic and Maxwell Problems, first ed, CRC Press, Boca Raton, FL, 2007.
[7] L. Demkowicz, W. Rachowicz, Ph. Devloo, A fully automatic *hp*-adaptation, J. Sci. Comput. 17 (2002) 117–142.
[8] J. Donea, A. Huerta, Finite Element Methods for Flow Problems, first ed, Willey, New York, 2003.
[9] K. Gerdes, D. Schötzau, hp-Finite element simulations for Stokes flow – stable and stabilized, Finite Elements Anal. Design 33 (1999) 143–165.
[10] T.J.R. Hughes, L.P. Franca, A new FEM for computational fluid dynamics: VII. The Stokes problem with various well-posed boundary conditions: symmetric formulations that converge for all velocity/pressure spaces, Comput. Methods Appl. Mech. Engrg. 65 (1987) 85–96.

[11] T.J.R. Hughes, L.P. Franca, M. Balestra, A new FEM for computational fluid dynamics: V. Circumventing the Babuśka–Brezzi Condition: a stable Petrov–Galerkin formulation of the Stokes problem accomodating equal-order interpolations, Comput. Methods Appl. Mech. Engrg. 59 (1986) 85–99.
[12] K.E. Jansen, S.S. Collis, Ch. Whithing, F. Shakib, A better consistency for low-order stabilized finite element methods, Comput. Methods Appl. Mech. Engrg. 174 (1997) 153–170.
[13] A.M. Maniatty, L. Liu, O. Klaas, M.S. Shephard, Stabilized finite element method for viscoplastic flow: formulation and a simple progressive solution strategy, Comput. Methods Appl. Mech. Engrg. 190 (2001) 4609–4625.
[14] P.J. Matuszyk, K. Boryczko, A Parallel Preconditioning for the Nonlinear Stokes Problem, Parallel Processing and Applied Mathematics, in: R. Wyrzykowski, J. Dongarra, N. Meyer, J. Waśniewski (Eds.), Proceedings of the 6th International Conference, LNCS 3911, Springer, Poznań, 2006, pp. 534–541.
[15] M. Paszyński, J. Kurtz, L. Demkowicz, Parallel fully automatic *hp*-adaptive 2D finite element package, Comput. Methods Appl. Mech. Engrg. 195 (7–8) (2006) 711–741.
[16] W. Rachowicz, D. Pardo, L. Demkowicz, Fully automatic hp-adaptivity in three dimensions, Comput. Methods Appl. Mech. Engrg. 195 (37–40) (2006) 4816–4842.